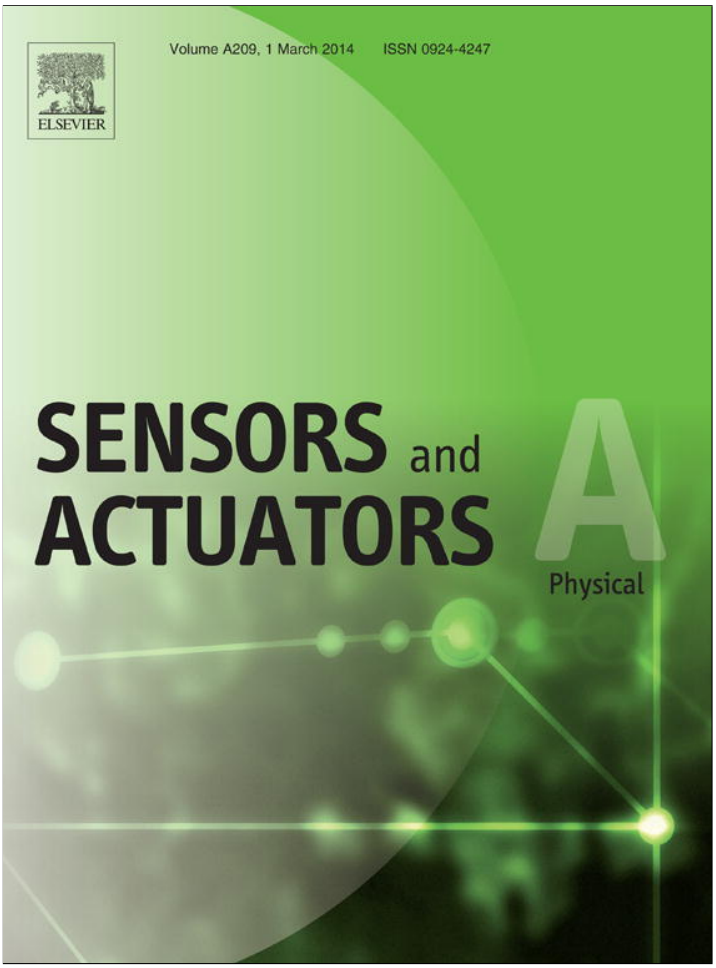

Sensors and Actuators A 209 (2014) 100–106

Contents lists available at ScienceDirect

Sensors and Actuators A: Physical

journal homepage: www.elsevier.com/locate/sna

Crawling microrobot actuated by a magnetic navigation system in tubular environments

Jaekwang Nam, Seungmun Jeon, Seungjoo Kim, Gunhee Jang*

PREM, Department of Mechanical Engineering, Hanyang University, 17 Haengdang-dong, Seongdong-gu, Seoul 133-791, Republic of Korea

ARTICLE INFO

Article history:
Received 24 August 2013
Received in revised form 16 January 2014
Accepted 16 January 2014
Available online 25 January 2014

Keywords:
Microrobot
Crawling
Tubular
Magnetic
Asymmetric friction
Human blood vessel

ABSTRACT

This paper proposes a crawling microrobot that can effectively navigate and anchor in various tubular environments including human blood vessels and pipes. The microrobot is a multibody structure comprising independently rotatable magnetic bodies with flexible legs and connecting rods. It can resist gravity and fluidic drag forces due to the moving mechanism using asymmetric friction force at the contact point between the leg and wall of the tube. Since the oscillating magnetic field generated by a magnetic navigation system (MNS) can induce oscillating motion of the microrobot, forward and backward crawling motions of the microrobot can be generated by controlling the currents in the MNS. This paper also proposes a methodology to effectively generate a three-dimensional (3D) oscillating magnetic field for the precise manipulation of the microrobot in a 3D tubular environment. Experiments in various environments were performed to verify the proposed microrobot.

1. Introduction

Occlusive vascular disease is a process in which arteries throughout the body become progressively narrower and eventually completely blocked. Although modern medical technology has made much progress, deaths from occlusive vascular diseases are rapidly increasing [1]. One common treatment for vascular occlusive diseases is using a catheter with a stent to unclog or enlarge clogged blood vessels [2]. However, even experienced medical doctors have difficulty controlling catheters in twisted and bent blood vessels. Microrobots manipulated by an electric or magnetic control system have been investigated as a promising alternative to conventional treatments.

Several types of swimming microrobots in fluidic environments have been investigated. Some researchers have studied swimming microrobots that utilize oscillating motions [3–7]. Guo et al. developed a microrobot that was composed of a driving fin, swam like a fish, and was powered by an oscillating magnetic field [3]. S. Sudo et al. investigated the swimming mechanism of a microrobot in a viscous liquid [4]. Valdastri et al. proposed a microrobot that swam like a jellyfish and was actuated by a DC motor using a wireless electric control system [5]. Kim et al. proposed a microrobot that swam like a tadpole and was actuated by an ionic polymer-metal composite actuator [6]. Liu et al. developed a microrobot driven by the vibration of a giant magnetostrictive thin film using an alternative magnetic field [7]. Other researchers have studied swimming microrobots that incorporate rotational motion [8,9]. Jeong et al. developed a helical microrobot manipulated by a rotating magnetic field and a magnetic gradient, and this microrobot was able to generate a drilling motion in a fluidic environment [8]. Pan et al. proposed a hybrid microrobot using a rotating and oscillating magnetic field [9]. Although these swimming microrobots are simple and suitable for static fluidic environments, additional control methodologies are required to stably manipulate the microrobot in a pulsatile fluidic environment, such as the blood stream in a coronary artery. Jeon et al. proposed a methodology to stabilize the undesired oscillating motion of a magnetic microrobot in a pulsatile flow by considering the electromagnetic transfer function of a magnetic navigation system (MNS). This system can reduce the oscillating motion of a magnetic microrobot induced by pulsatile flow, but it requires a sensor to measure the velocity of the blood flow to determine the drag force of the microrobot [10]. On the other hand, several researchers have developed multibody robots that rely on friction forces exerted on the robots [11–15]. These robots can generate stable motions by making contact with external environments such as the wall of a tube. Zimmerman et al. investigated vibration-driven electric robots using asymmetric friction force [11]. Kim et al. proposed an earthworm-like electric microrobot that uses a shape memory alloy and a microneedle to clamp onto the contact surface [12]. Sun et al. developed an electric microrobot that uses a piezoelectric actuator in a small pipe. This microrobot can move along the pipe with the legs supported by

* Corresponding author. Tel.: +82 2 2220 0431; fax: +82 2 2292 3406.
E-mail address: ghjang@hanyang.ac.kr (G. Jang).

0924-4247/$ – see front matter © 2014 Elsevier B.V. All rights reserved.
http://dx.doi.org/10.1016/j.sna.2014.01.025

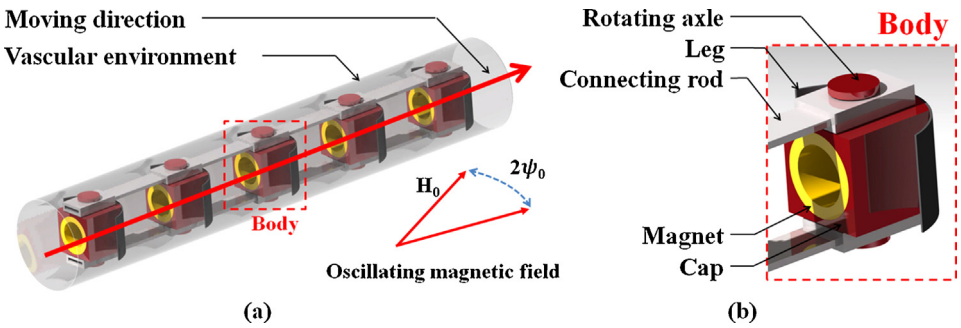

Fig. 1. (a) Structure of the crawling microrobot. (b) Detailed view of the body of the crawling microrobot.

the wall of the pipe [13]. Kim et al. developed magnetic walking and creeping robots using amphibious and snake-like locomotion, respectively [14,15]. However, some of these robots carry an electrical system that requires batteries or tethered wires [11–13], and the other robots are structurally not suitable for tubular environments such as human blood vessels [14,15].

We propose a crawling microrobot consisting of several permanent magnets, flexible legs, and connecting rods, as shown in Fig. 1. A magnetic field generated by an external coil system energizes the microrobot to perform various motions in complex tubular environments. An oscillating magnetic field can produce an oscillating motion of the microrobot, and the resulting asymmetric friction forces at the contact points between the legs and the wall of the tube make the microrobot crawl forward or backward. This friction force can also stably anchor the microrobot against disturbing forces such as gravitational and pulsatile fluidic drag forces. The magnetic and mechanical torques of the microrobot are analyzed to investigate the effective driving mechanism of the microrobot. We also propose a methodology to effectively generate three-dimensional (3D) crawling motions of the microrobot. Experiments in various environments were performed to verify the effectiveness of the proposed microrobot.

2. Development of a crawling microrobot

2.1. Structure of the crawling microrobot

The proposed crawling microrobot comprises a multibody structure, as shown in Fig. 1. Each body is composed of a permanent magnet, cap, rotating axle, and leg connected by connecting rods. Each body of the proposed microrobot is rotatable with respect to the rotating axle. A ring-type permanent magnet magnetized along the permanent magnet is inserted into the cap, and an inner hole allows fluid flow to reduce drag. Since the legs of the microrobot are made of a long elastomer to support the wall of a tube, the microrobot cannot only crawl through tubes of various sizes but also anchor stably under various disturbing forces.

2.2. Moving principle of the crawling microrobot

The proposed microrobot utilizes asymmetric friction forces generated at the contact points between the legs and tube to generate a crawling motion. When a body of the microrobot is rotated counter-clockwise, a positive friction force is generated at the upper leg and a negative friction force is generated at the lower leg, as shown in Fig. 2(a). Since the positive friction force is greater than the negative friction force due to the different contact angles [16], the net positive friction force of the microrobot can make the microrobot move forward. Assuming that the microrobot moves Δx along the x-axis when it is rotated counter-clockwise from $-\psi_0$ to ψ_0, the microrobot also moves Δx along the x-axis when rotated clockwise from ψ_0 to $-\psi_0$, as shown in Fig. 2(b). Repeated motions in Fig. 2(a) and (b) can generate continuous forward crawling motion of the microrobot. Backward crawling motion can be generated by the same sequence after the turning motion of the microrobot in the opposite direction. Since the principle of manipulation is based on the friction forces, the rectilinear movement of the microrobot can be achieved by controlling the rotational motion of the microrobot unless external disturbing forces are greater than the maximum frictional force.

2.3. Generation of driving torque for the crawling motion

The oscillating motion of a microrobot can be obtained by applying rotational magnetic torque to the microrobot. The effective torque (net torque) of the microrobot to generate the rotational motion along its rotating axis can be defined as follows.

$$\mathbf{T_{net}} = \mathbf{T_e} - \mathbf{T_i} - \mathbf{T_r} \tag{1}$$

where $\mathbf{T_{net}}$, $\mathbf{T_e}$, $\mathbf{T_i}$, and $\mathbf{T_r}$ are the net torque of the microrobot, external magnetic torque, internal magnetic torque, and resistive torque generated by asymmetric friction force and drag force, respectively. In Eq. (1), $\mathbf{T_e}$ can only be controlled by the external magnetic field. The external magnetic torque applied to the body can be expressed as follows.

$$\mathbf{T_e} = \mu_0 \mathbf{m} \times \mathbf{H_e} \tag{2}$$

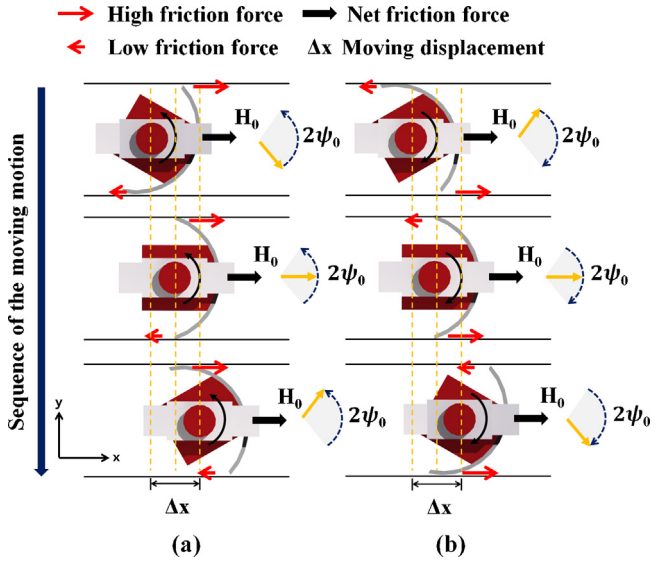

Fig. 2. Rectilinear forward movement of the crawling microrobot induced by (a) counter-clockwise rotating motion and (b) clockwise rotating motion.

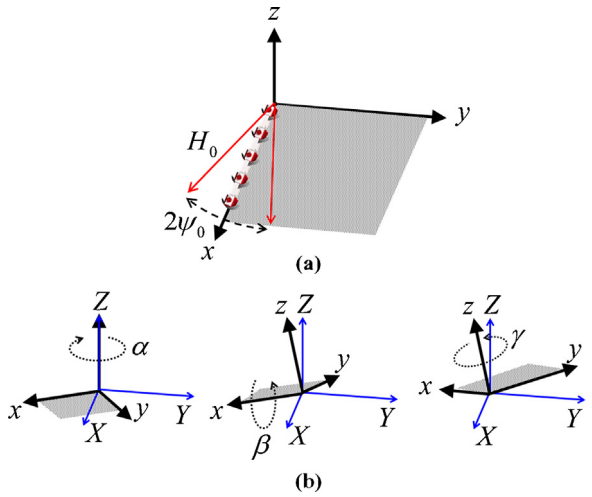

Fig. 3. (a) Local coordinates *x*, *y*, and *z* fixed to the microrobot and the external oscillating magnetic field along *x*-axis in the *xy* plane. (b) Rotation sequence of Euler angle (*z*–*x*–*z*) from the local coordinates to the global coordinates *X*, *Y*, and *Z*.

where μ_0, $\mathbf{m}$, and $\mathbf{H_e}$ are the permeability of free space, the magnetic moment of the body, and the external magnetic intensity, respectively.

The crawling motion of a microrobot can be assumed to be piecewise one-dimensional motion with the consideration that the microrobot can only move forward or backward along the tube. In this paper, that direction is defined as the local *x*-direction, and the Euler angle is utilized to transform from the required magnetic field in local coordinates to the controlled current of the magnetic navigation system in global coordinates. By introducing the local coordinates that are fixed to the microrobot, as shown Fig. 3(a), the local external magnetic field required to generate an *x*-directional crawling motion of the microrobot can be expressed as follows.

$$\mathbf{H_e^{local}} = H_0 \begin{bmatrix} \cos\psi_e & \sin\psi_e & 0 \end{bmatrix}^T \tag{3}$$

$$\psi_e = \psi_0 \sin(2\pi f t) \tag{4}$$

where H_0, ψ_0, and f are the amplitude, oscillating angle, and frequency of the oscillating external magnetic intensity, respectively. The external magnetic field with respect to the global coordinate can be calculated using the coordinate transformation matrix derived from the Euler angle, as shown in the following equation.

$$\mathbf{H_e} = \begin{bmatrix} c_\alpha c_\gamma - c_\beta s_\alpha s_\gamma & -c_\alpha s_\gamma - c_\beta c_\gamma s_\alpha & s_\alpha s_\beta \\ c_\gamma s_\alpha + c_\alpha c_\beta s_\gamma & c_\alpha c_\beta c_\gamma - s_\alpha s_\gamma & -c_\alpha s_\beta \\ s_\beta s_\gamma & c_\gamma s_\beta & c_\beta \end{bmatrix} \mathbf{H_e^{local}} \tag{5}$$

where c_i and s_i are the sine and cosine function of the *i*th angle, respectively, and subscripts α, β, and γ represent the three Euler angles. Fig. 3(b) shows the rotation sequence of the Euler angle.

The proposed microrobot is affected not only by the external magnetic field but also by the internal magnetic field generated by the adjacent magnets within the microrobot. Assuming that the microrobot has an odd number (n) of identical magnets, as shown in Fig. 4, the internal magnetic intensity of the microrobot generated at the body of the microrobot located at the center (magnet 0) of the adjacent body (magnet 1) can be calculated by using a dipole model as follows [17].

$$\mathbf{H}_{10} = \frac{[3\hat{\mathbf{r}}_\mathbf{m}(\mathbf{m}\cdot\hat{\mathbf{r}}_\mathbf{m}) - \mathbf{m}]}{4\pi r_m^3} \tag{6}$$

where $\mathbf{m}$, $\hat{\mathbf{r}}_\mathbf{m}$, and r_m are the magnetic moment of the magnet and the unit vector from magnet 1 to magnet 0 and its magnitude, respectively, as shown in Fig. 4. Assuming that the bodies of the

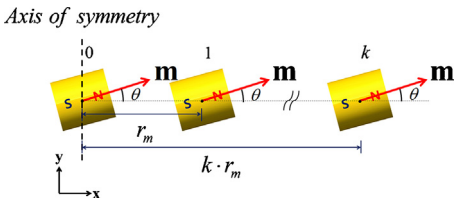

Fig. 4. Simultaneous rotating motion of n identical magnets of the crawling microrobot.

microrobot are spaced at identical distances and that each magnet has the same angle of θ with respect to the connecting rod, the overall internal magnetic field and the internal magnetic torque exerted on magnet 0 can be expressed as follows.

$$\mathbf{H_i} = 2\mathbf{H}_{10} \sum_{k=1}^{(n-1)/2} \frac{1}{k^3} \tag{7}$$

$$\mathbf{T_i} = \mu_0 \mathbf{m} \times \mathbf{H_i} \tag{8}$$

Since the magnets of the microrobot are magnetized along the axial direction, the internal magnetic fields tend to align the magnets straight along the *x*-axis. Therefore, the external magnetic torque in Eq. (2) should be strong enough to overcome the internal magnetic torque in Eq. (8), expressed as follows.

$$\left|\mu_0 \mathbf{m} \times \mathbf{H_e}\right| \geq \left|\mu_0 \mathbf{m} \times 2\mathbf{H}_{10} \sum_{k=1}^{(n-1)/2} \frac{1}{k^3}\right| \tag{9}$$

The minimum value of r_m can be calculated from the equality condition of Eq. (9). When n is infinitely large, r_m can be determined as follows.

$$r_m^{\min} = \sqrt[3]{\frac{9|\mathbf{m}|}{10\pi H_e}} \tag{10}$$

Fig. 5 shows the variations of $\mathbf{T_i}/|\mathbf{T_e}|$ according to the variations of θ and r_m. It shows that the maximum magnitude of $\mathbf{T_i}$ is equal to $\mathbf{T_e}$ when r_m is equal to $r_m^{\min}$. In this case, the microrobot has no extra torque to overcome $\mathbf{T_r}$, so r_m should be chosen to be larger than $r_m^{\min}$. In a real operating environment, $\mathbf{T_e}$ should be greater than the summation of $\mathbf{T_i}$ and $\mathbf{T_r}$ as shown in Eq. (1). The maximum amplitude of $\mathbf{T_r}$ can be experimentally determined by measuring the minimum value of r_m which allows the microrobot to be rotated by the given external magnetic field in a tubular environment.

The required external magnetic field can be calculated to generate the crawling motion of the microrobot in a 3D complex tubular environment by using Eqs. (1)–(10). The navigating direction of the microrobot can also be controlled using Eqs. (1)–(10) in the entering direction of a bifurcated branch of the tubular environment.

In this study, we used a MNS to effectively generate the external magnetic field. Generally, a uniform coil such as a Helmholtz coil can generate a uniform magnetic field along its axis [18]. Thus, a 3D uniform magnetic field can be similarly generated by using an MNS composed of three orthogonal pairs of uniform coils without the mechanical motion of the MNS. Fig. 6 shows an MNS composed of one Helmholtz coil and two uniform saddle coils that can effectively generate a 3D oscillating magnetic field within a compact structure [19].

The magnetic field intensity generated by each coil of the MNS can be expressed in terms of the number of turns, size, and current, as shown in the following equation [19].

$$\mathbf{H_e} = \begin{bmatrix} d_h & d_{uy} & d_{uz} \end{bmatrix}^T \tag{11}$$

$$d_h = \frac{(4/5)^{3/2} i_h}{r_h}, \quad d_{uy} = \frac{0.6004 i_{uy}}{r_{uy}}, \quad d_{uz} = \frac{0.6004 i_{uz}}{r_{uz}} \tag{12}$$

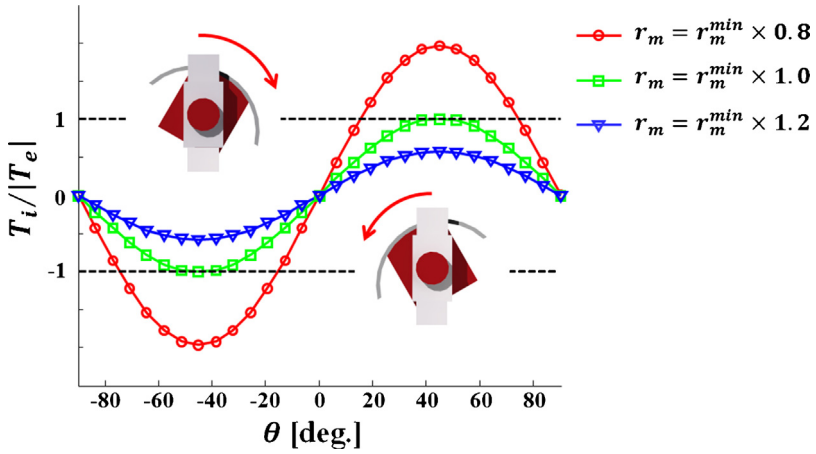

Fig. 5. Magnitude variations in $\mathbf{T_i}/|\mathbf{T_e}|$ according to the variations in θ and r_m.

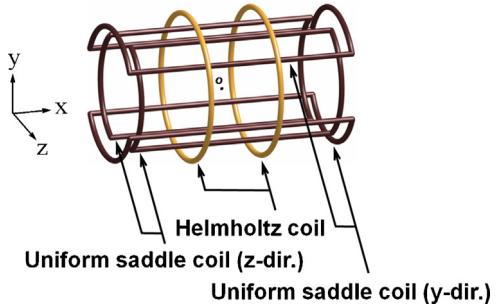

Fig. 6. The MNS composed of one Helmholtz coil and two uniform saddle coils to generate a 3D external magnetic field.

where i_k and r_k are the current and radius of the kth coil, and the subscripts h, uy, and uz represent the Helmholtz coil, y-directional uniform saddle coil, and z-directional uniform saddle coil, respectively. Therefore, the crawling motion of the microrobot can be effectively controlled by controlling the currents of the MNS.

3. Results and discussion

We constructed an experimental setup to verify the locomotion ability of the proposed crawling microrobot. We prototyped the microrobot with the specifications as shown in Table 1. The prototyped microrobot has 4 identical bodies, and each body comprises a ring-type neodymium magnet, cap, flexible leg, and connecting rod as shown in Fig. 7. For the prototyped microrobot, r_m^{min} was calculated as 15 mm from Eq. (9) under an external magnetic field with a magnitude of 14 mT. We observed that the microrobot with more than 14 mm between magnets was able to rotate under the same external magnetic field, which matches well with the calculated result. We also determined the maximum amplitude of $\mathbf{T_r}$ by measuring the minimum value of r_m, which allows the microrobot to be

Table 1
Main design variables of the prototype crawling microrobot.

Component	Material	Size (mm)	
Leg	Silicon	L_w	40
Cap	Ultraviolet curable acrylic plastic	C_h	13
Rotating axle	Ultraviolet curable acrylic plastic	R_h	1.6
Connecting rod	Ultraviolet curable acrylic plastic	–	–
Magnet	NdFeB (magnetization: 954.93 kA/m, magnetic moment: 0.144 A m^2)	M_h	8
		M_o	7
		M_i	5

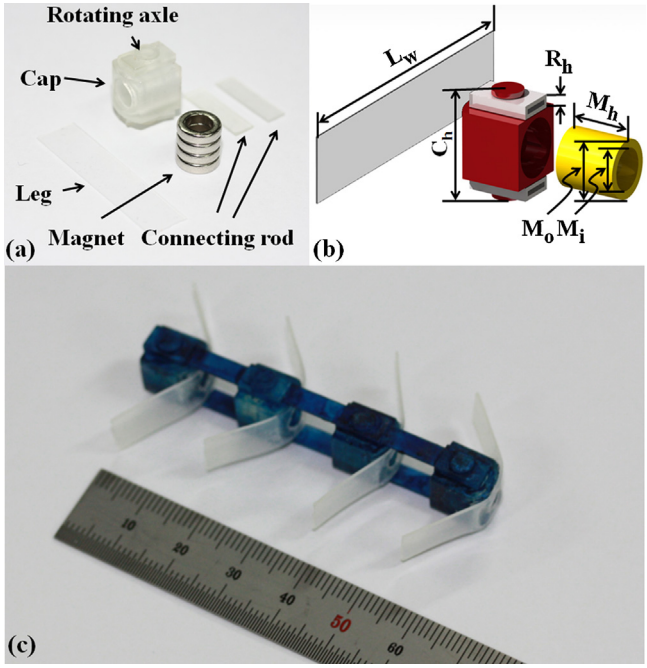

Fig. 7. Structure of the crawling microrobot. (a) Components of the crawling microrobot. (b) Specifications of the components of the crawling microrobot. (c) Assembled crawling microrobot with four bodies.

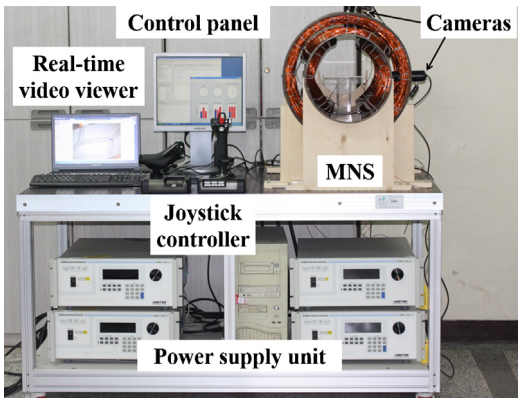

Fig. 8. Experiment setup to control the crawling motion of the microrobot.

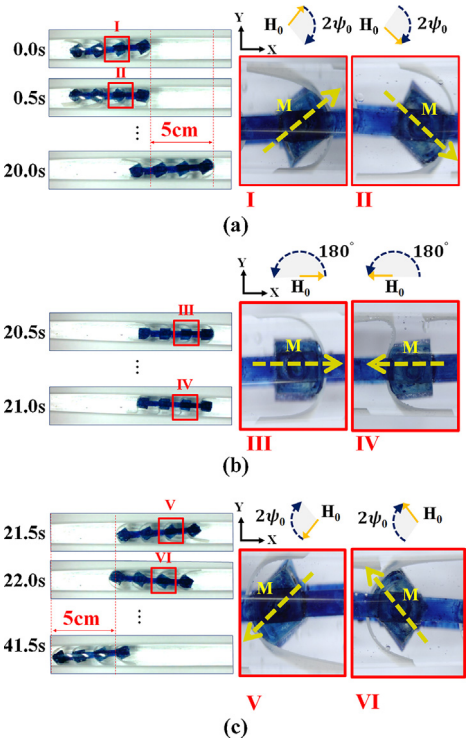

Fig. 9. Forward and backward motion of the crawling microrobot at an oscillating frequency of 1 Hz and oscillating angle of 60°. (a) Forward crawling motion (0.0–20.0 s). (b) Turning motion to reverse the moving direction (20.5–21.0 s). (c) Backward crawling motion (21.5–41.5 s).

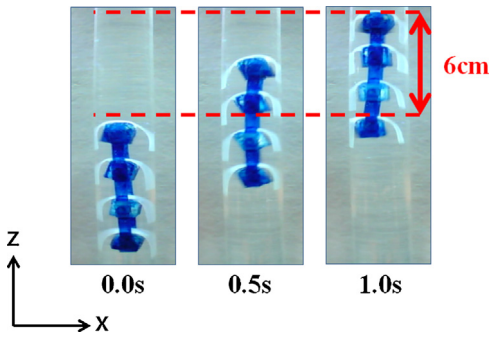

Fig. 11. Vertical crawling motion of the microrobot along a tube with a diameter of 18 mm (oscillating frequency: 15 Hz, oscillating angle: 90°, magnetic field: 14 mT).

rotated by the external magnetic field in a tubular environment. In dry transparent acrylic tubes with diameters of 18 mm and 21 mm, the minimum values of r_m were measured as 18 mm and 17 mm, and the maximum amplitudes of $\mathbf{T_r}$ were then determined to be 0.74 mN m and 0.50 mN m, respectively, using Eqs. (1), (2) and (10). Since the friction force in a dry environment is generally greater than that in a fluidic environment, the prototyped microrobot can be applied to both dry and fluidic conditions.

Fig. 8 shows the experimental setup consisting of an MNS and control system to control the crawling motion of the microrobot. The MNS can generate a 3D oscillating external magnetic field with a maximum magnitude of 14 mT that can be simply controlled by a joystick interface. The motion of the microrobot is tracked by two orthogonal cameras.

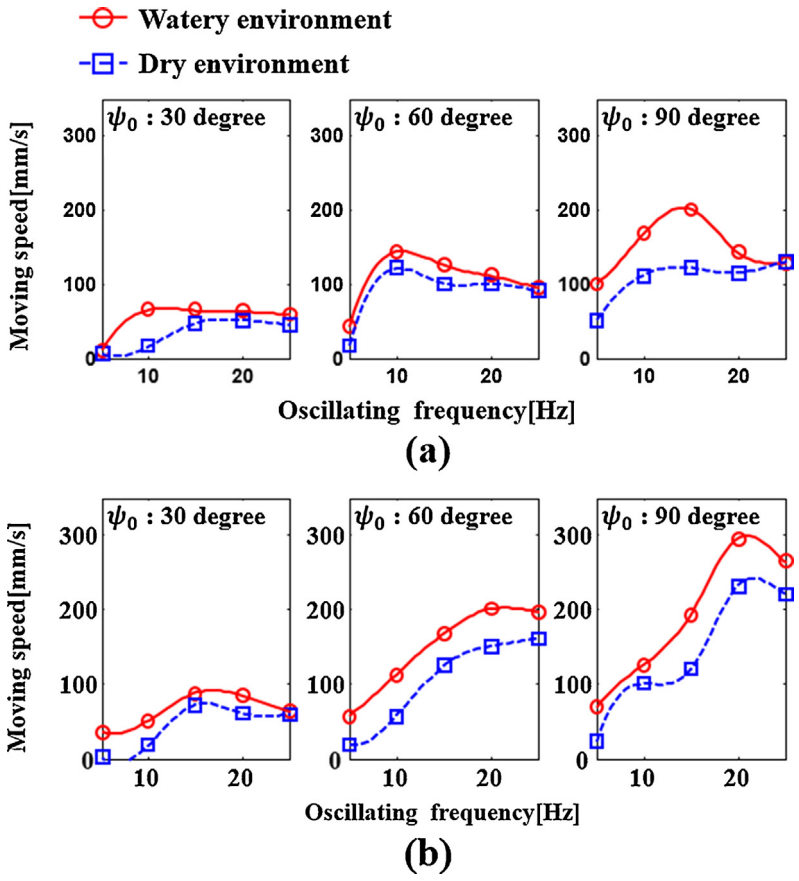

Fig. 10. Experimentally measured moving speed of the crawling microrobot due to the oscillating frequency, oscillating angle, tube diameter, and fluidic condition. (a) Moving speed of the crawling microrobot along a tube with a diameter of 18 mm. (b) Moving speed of the crawling microrobot along a tube with a diameter of 21 mm.

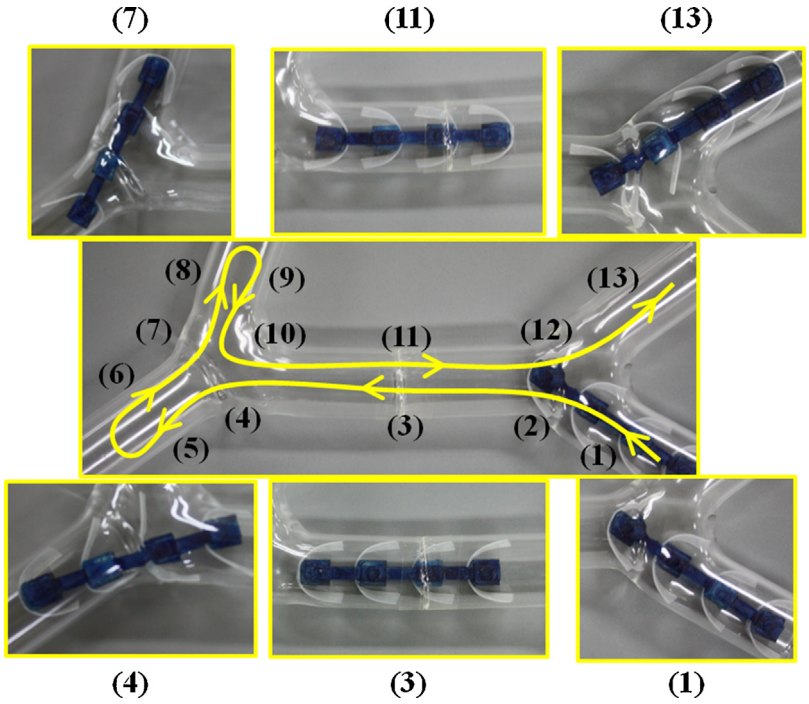

Fig. 12. Crawling motion of the microrobot in a bifurcated tube. The microrobot moves sequentially according to the marked number (starting position: 1, final position: 13).

Table 2
Fastest moving speed of the crawling microrobot along horizontal and vertical watery tubes.

Driving condition			Moving speed (mm/s)	
Tube diameter (mm)	Oscillating frequency (f, Hz)	Oscillating angle (ψ_0,°)	Horizontal tube	Vertical tube
18	15	90	200.00	60.00
21	20	90	294.12	90.91

Fig. 9(a) shows the crawling motion of the microrobot in a watery tube with a diameter of 18 mm. The microrobot is driven forward by an *X*-directional oscillating magnetic field. Fig. 9(b) shows the turning motion of the microrobot as it is rotated by a rotating magnetic field. After the turning motion, the microrobot crawls backward due to the negative *X*-directionally oscillating external magnetic field, as shown in Fig. 9(c).

Fig. 10 shows the moving speed of the microrobot with different oscillating frequencies, oscillating angles and tube diameters in watery and dry conditions. At low oscillating frequencies, the moving speeds of the microrobot are proportional to both the oscillating angles and oscillating frequencies because the microrobot simultaneously oscillates with the synchronization of the external magnetic field. However, the moving speed of the microrobot decreases at high oscillating frequencies due to the step-out phenomenon in which the microrobot cannot synchronize with the external magnetic field due to the inertia effect. The microrobot in the watery tube moves faster than the microrobot in the dry tube due to the smaller friction forces.

To show the vertical locomotion ability of the proposed microrobot, the crawling motion of the microrobot in a watery vertical tube is then demonstrated, as shown in Fig. 11. This shows that the microrobot can crawl upward along the vertical tube but its speed is slower than that along the horizontal tube. The fastest moving speed of the prototyped microrobot in both horizontal and vertical watery tubes is shown in Table 2. Due to the frictional forces generated at the contact point between the legs of the microrobot and the wall of the tube, the microrobot can still anchor vertically at the resting point under the gravitational and fluidic drag forces even after the external magnetic field is removed. This ability would be greatly useful when the microrobot is to be applied in harsh environments such as the inevitable pulsatile flows in human blood vessels [10].

The crawling motion of the microrobot was also demonstrated in a bifurcated tube as shown in Fig. 12. The moving speed and direction of the microrobot were stably and selectively manipulated to move forward and backward and to choose which branch to enter.

4. Conclusion

This research developed a crawling microrobot that can stably move along a tube by using the asymmetric friction force originating from an oscillating external magnetic field. The asymmetric friction force both propels and anchors the microrobot in a 3D fluidic tubular environment. This research could further be extended to manipulate a multi-functional microrobot precisely for various applications, such as drug delivery or stent installation, in the harsh environment of human blood vessels as well as to solve the localization problem, which is to determine the microrobot's position in the human body.

Acknowledgements

This work was supported by a grant from the National Research Foundation of Korea (NRF), funded by the Korean Government (MEST) (No. 2012R1A2A1A01).

References

[1] D. Lloyd-Jones, et al., Heart disease and stroke statistics, American Heart Association & American Stroke Association 119 (2009) 480–486.

[2] S. Saito, S. Tanaka, Y. Hiroe, Y. Miyashita, S. Takahashi, S. Satake, K. Tanaka, Angioplasty for chronic total occlusion by using tapered-tip guidewires, Catheterization and Cardiovascular Interventions 59 (3) (2003) 305–311.

[3] S. Guo, Q. Pan, M.B. Khamesee, Development of a novel type of microrobot for biomedical application, Microsyst Technologies 14 (3) (2008) 307–314.

[4] S. Sudo, S. Segawa, T. Honda, Magnetic swimming mechanism in a viscous liquid, Journal of Intelligent Material Systems and Structures 17 (8–9) (2006) 729–736.

[5] P. Valdastri, E. Sinibaldi, S. Caavaro, G. Tortora, A. Menciassi, P. Dario, A novel magnetic actuation system for miniature swimming robots, IEEE Transactions on Robotics 27 (4) (2011) 769–779.

[6] B. Kim, D. Kim, J. Jung, J. Park, A biomimetic undulatory tadpole robot using ionic polymer–metal composite actuators, Smart Materials and Structures 14 (6) (2005) 1579–1585.

[7] W. Liu, X. Jia, F. Wang, Z. Jia, An in-pipe wireless swimming microrobot driven by giant magnetostrictive thin film, Sensors and Actuators A: Physical 160 (1–2) (2010) 101–108.

[8] S. Jeong, H. Choi, K. Cha, J. Li, J. Park, S. Park, Enhanced locomotive and drilling microrobot using precessional and gradient magnetic field, Sensors and Actuators A: Physical 171 (2) (2011) 429–435.

[9] Q. Pan, S. Guo, T. Okada, Development of a wireless hybrid microrobot for biomedical applications, Proceedings of the IEEE/RSJ International Conference on intelligent Robots and Systems (2010) 5768–5773.

[10] S. Jeon, G. Jang, J. Choi, S. Park, J. Park, Precise manipulation of a microrobot in the pulsatile flow of human blood vessels using magnetic navigation system, Journal of Applied Physics 109 (7) (2011) 07B316.

[11] K. Zimmerman, I. Zeidis, N. Bolotnik, S. Jatsun, Dynamics of mobile vibration-driven robots, SYROM 2009, in: Proceedings of the 10th International Symposium on Science of Mechanism and Machines, 2009, pp. 465–477.

[12] B. Kim, M. Lee, Y. Lee, Y. Kim, G. Lee, An earthworm-like microrobot using shape memory alloy actuator, Sensors and Actuators A: Physical 125 (2) (2006) 429–437.

[13] L. Sun, Y. Zhang, P. Sun, Z. Gong, Study on robots with PZT actuator for small pipe, in: Proceedings of 2001 International Symposium on Micromechatronics and Human Science, 2001, pp. 149–154.

[14] S. Kim, J. Lee, S. Hashi, K. Ishiyama, Oscillatory motion-based miniature magnetic walking robot actuated by a rotating magnetic field, Robotics and Autonomous Systems 60 (2) (2012) 288–295.

[15] S. Kim, S. Hashi, K. Ishiyama, Magnetic actuation based snake-like mechanism and locomotion driven by rotating magnetic field, IEEE Transactions on Magnetics 47 (10) (2011) 3244–3247.

[16] N. Antoni, J.-L. Ligier, P. Saffré, J. Pastor, Asymmetric friction: modelling and experiments, International Journal of Engineering Science 45 (2–8) (2007) 587–600.

[17] K.W. Yung, P.B. Landecker, D.D. Villani, An analytic solution for the force between two magnetic dipoles, Physical Separation in Science and Engineering 9 (1) (1998) 39–52.

[18] S. Jeon, G. Jang, H. Choi, S. Park, Magnetic navigation system with gradient and uniform saddle coils for the wireless manipulation of micro-robots in human blood vessels, IEEE Transactions on Magnetics 46 (6) (2010) 1943–1946.

[19] S. Jeon, G. Jang, H. Choi, S. Park, J. Park, Magnetic navigation system for the precise helical and translational motions of a microrobot in human blood vessels, Journal of Applied Physics 111 (7) (2012) 07E702.

Biographies

Jaekwang Nam is a graduate student in the department of Mechanical Engineering at Hanyang University, Seoul, Korea. He received his B.S. in Mechanical Engineering from Hanyang University in 2011. His reaseach interests are various structures of the mictrorobots performing multifunction in human blood vessels by magnetic navigation system.

Seungmun Jeon received his B.S. in Mechanical Engineering from Hanyang University, Seoul, Korea in 2008. He joined the Precision Rotating Electromechanical Machine Laboratory (PREM) at Hanyang University in 2007 as a Ph.D. student. His fields of interests are analysis, design, and control of biomedical microrobots and electromagnetic systems.

Seungjoo Kim is a graduate student in the department of Mechanical Engineering at Hanyang University, Seoul, Korea. He received his B.S.(2013) degree from the department of Mechanical Engineering from Hanyang University, Seoul, Korea. His research interests are microrobot and control.

Gunhee Jang received the B.S. in Mechanical Engineering from Hanyang University, Seoul, Korea in 1984, the M.S. in Mechanical Engineering from Korea Advanced Institute of Science and Technology (KAIST), Seoul, Korea in 1986 and the Ph.D. in Mechanical Engineering from University of California, Berkeley, USA in 1993. He is a professor in the Department of Mechanical Engineering and the director of the Precision Rotating Electromechanical Machine Laboratory (PREM) in Hanyang University, Seoul, Korea. His current research is focused on the microrobot actuated by magnetic navigation system, electromechical systems such as motors and actuators. He has authored or coauthored over 230 articles published in journals and conferences in his field and over 20 patents including several international patents.